Non-invasive diagnosis of solid electrolyte interphase and charge transfers resistances for degraded lithium-ion batteries

Fernanda Vendrame, Nicolas Damay, Houssam Rabab, Christophe Forgez, Marie Sayegh

Non-invasive diagnosis of solid electrolyte interphase and charge transfers resistances for degraded lithium-ion batteries

Fernanda Vendrame[a,b], Nicolas Damay[a,*], Houssam Rabab[a], Christophe Forgez[a], Marie Sayegh[b]

[a] *Université de Technologie de Compiègne, Roberval (Mechanics, Energy and Electricity) Centre de recherche Royallieu, CS 60319, 60203 Compiègne Cedex, France*
[b] *Safran Electrical & Power 70-80 Rue Auguste Perret, 94000 Créteil, France*

Abstract

Modeling the electrical behavior of cells is often complex because several parameters have to be determined simultaneously, which may lead to inconsistencies and inaccuracies. In the present paper, we modeled the "surface resistance" by using a method based on rules of dependence, already presented in the literature, which makes it possible to separate the contributions of the SEI (Solid Electrolyte Interphase) layer and the charge transfers as a function of the temperature and the current. A physical model is able to provide a consistent estimate of the surface resistance values at untested operating points. We transposed this model to NCA ($LiNi_xCo_yAl_{1-x-y}O_2$) and NMC-622 ($LiNi_{0.6}Mn_{0.2}Co_{0.2}O_2$) / graphite+Si cells and we characterized them for different states of health (SOH). For a SOH of 87%, we found that the charge transfers resistance was multiplied at least by 5.8, while the SEI resistance was multiplied at least by 1.5. As the cell ages, the proposed model should be easier to recalibrate than lookup tables. For that, we propose two methods, one that provides more detailed and accurate results and one that is more practical from an engineering point of view.

Keywords: lithium-ion, battery, diagnosis, electrical model, Solid Electrolyte Interphase, charge transfer

1. Introduction

An accurate model of lithium-ion cells is a key element to understand the impact of operating conditions on their behavior, which may be very useful for determining crucial information such as the cell state of charge (SOC), state of health, among other indicators.

There are multiple ways of representing the behavior of a cell, such as an electrochemical model [1, 2, 3, 4], a data-driven model [5] or an equivalent circuit model (ECM) [6, 7, 8, 9]. In this study, we need a model that represents the overall behavior of the cell in a physically consistent way. Data-driven models can be very effective in representing the overall behavior, but do not necessarily have physical meaning. Electrochemical models are physics-based and naturally take into account the non-linearities of the cell behavior, but are better suited to describe local phenomena. This is why we will develop our work using an ECM.

The ECM parameters depend on many factors, such as temperature, current, state of charge and state of health [9, 10, 11]. Many tests are usually necessary in order to obtain the values of these parameters at different operating conditions and the results can be presented in the form of lookup tables, which will be all the more precise as the tests are numerous. However, this method presents three problems: (1) it is difficult to recalibrate these lookup tables as the battery ages, (2) a linear interpolation between two points may give an inaccurate value of the parameter and (3) the parameters values are usually found by using optimization algorithms which usually provide solutions that are mathematically coherent, but are not necessarily physically coherent.

To address these issues, our team [12] developed a method for studying one of the parameters of the electrical model, namely the surface resistance, which establishes some rules of dependence, making it possible to find a physically coherent equation of this parameter as a function of current and temperature. This method eliminates the problem of interpolation, reduces the number of tests required and allows physical information to be extracted from the parameter. Because the model of this parameter is physically based, it should remain consistent when the battery ages. More precisely, his governing equations are expected to remain the same, but his parameters value may change because of the internal degradations due to aging.

The effects of aging can be different depending on whether the cell was aged in cycling or calendar mode. Regarding cycling aging, Wong *et al.* [13, 14] found that during cycling aging, the application of high current rates contribute to the rapid formation of a high impedance film, which causes a drastic change in charge transfers kinet-

*Corresponding author
Email address: nicolas.damay@utc.fr (Nicolas Damay)

ics. A significant loss of capacity was observed, as well as a large increase in the charge transfers resistance and a mild growth of the SEI layer. Sabet *et al.* [15] studied NMC cells during cycling aging and observed an increase in charge transfers resistance. The main mechanisms identified were anode's and cathode's particle cracking, cathode dissolution and possibly CEI (Cathode-Electrolyte Interphase) layer growth. Regarding calendar aging, Stiaszny *et al.* [16] evaluated the impact of storing NCA cells at 60 °C at different SOC levels. They observed that the resistances of the SEI layer and the cathode charge transfers resistance increased. The growth of the SEI layer was even more drastic at higher SOC. Sabet *et al.* [15] observed that both SEI and charge transfers resistances increased for calendar aging.

In most of the mentioned works, the study of aging mechanisms is mainly based on EIS (Electrochemical Impedance Spectroscopy) test results [17, 18]. This method makes it possible to extract precious information about the effects of different aging conditions for different cell chemistries. However, it mainly gives information about what happens at near zero current, whereas the behavior of the cell changes significantly with increasing current. Besides, EIS does not always allow the different surface phenomena (i.e. SEI, charge transfers) to be distinguished due to their similar dynamics, especially at room temperature [19]. Our method fills these gaps as it is applicable to the entire range of currents that the cell can withstand and makes it possible to distinguish SEI and charge transfers contributions even when they have similar time constants. Some positive electrodes may also have a SEI that have a significant contribution such as Ni-rich cathodes [20, 21] and high-voltage $LiCoO_2$ (LCO) cathodes [22]. This study does not apply to batteries using these cathodes and is focused on batteries with a significant SEI only at their anodes.

The present paper has three main objectives. The first objective is to show that the method developed by our team [12] for modeling the surface resistance can be transposed to a NCA+NMC / graphite+Si cell, as it was originally developed using a LFP ($LiFePO_4$) / graphite cell. The second objective is to validate a new characterization protocol dedicated to the surface resistance, that is faster than in the previous study. The third objective is to demonstrate the model remains consistent for degraded lithium-ion cells and that it can hence be used as a efficient diagnosis tool for future aging studies.

In the next section, the electrical cell model is presented. Its structure is detailed, as well as the methods and experimental tests needed in order to obtain its parameters, with a characterization protocol that is faster than in the previous study [12]. Section 3 is focused on the surface resistance, which is one of the parameters of the electrical cell model. The physical laws that describe its behavior as a function of temperature (Arrhenius equation) and current (Butler-Volmer equation) are presented in order to identify the individual contributions of SEI layer and charge transfers phenomena. Finally, the results of this analysis are presented in section 4, followed by a discussion about the impact of aging over these two contributions and a comparison between our results and the literature. Some perspectives are also presented to guide the next steps of this research.

2. Battery model

2.1. Equivalent circuit model

The equivalent circuit model used in this study, represented in Fig. 1, is composed of the following elements:

- U_{oc}: a voltage source representing the OCV (open circuit voltage). This is the voltage of the cell in open circuit and at equilibrium.
- R_s: a series resistance representing all purely resistive contributions, such as electrolyte, current collectors, contact and pore resistances [17, 23].
- R_{surf}: a surface resistance related to the voltage drop between the surface of the active material and the electrolyte, due to charge transfers and SEI [12].
- $\tau_{surf} = R_{surf} \times C_{surf}$: a time constant related to the surface phenomena, which are associated with charge transfers, double layers and SEI. It represents a quick dynamic, usually inferior to 1 second.
- Z_{diff}: impedance related to the phenomena of lithium ions diffusion in the electrolyte and lithium atoms in both electrodes, having a slow dynamic, usually in the order of several minutes [24, 25]. This impedance can be represented by a series of n RC circuits, with $2n$ parameters. However, the diffusion resistances $R_{diff,i}$ and the diffusion time constants $\tau_{diff,i}$ of all the circuits can be calculated from a global value of R_{diff} and τ_{diff} ($R_{diff} \times C_{diff}$) using the following equations [12, 26]:

$$R_{diff,i} = \frac{R_{diff,1}}{(2i-1)^2} \tag{1}$$

$$C_{diff,i} = C_{diff} \tag{2}$$

$$\tau_{diff,i} = \frac{\tau_{diff,1}}{(2i-1)^2} \tag{3}$$

where

$$R_{diff,1} = \frac{R_{diff}}{\sum_{i=1}^{n} \frac{1}{(2i-1)^2}} \tag{4}$$

$$\tau_{diff,1} = \frac{\tau_{diff}}{\sum_{i=1}^{n} \frac{1}{(2i-1)^2}} \tag{5}$$

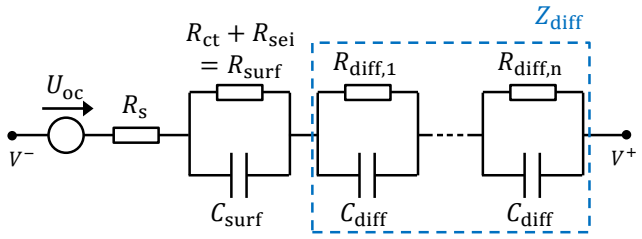

Figure 1: Equivalent circuit model

Once R_{surf} is identified, its behavior for different current rates and temperatures can be studied. Its dependence on SOC has not yet been analyzed, so it will not be addressed in the present paper. However, EIS (Electrochemical Impedance Spectroscopy) tests are a simple way to observe, for a given cell, whether the surface resistance depends strongly on SOC. Taking the cell used in this work as an example, its surface resistance varies very slightly between SOC 10% and 70%, so the proposed method could be applied to one SOC value within this range and to some values closer to 0% and 100% depending on the requirements of the application.

2.2. Experimental protocol

Three commercial cells Samsung 18650-25R were used for this study. These are NCA ($LiNi_xCo_yAl_{1-x-y}O_2$) and NMC-622 ($LiNi_{0.6}Mn_{0.2}Co_{0.2}O_2$) / graphite+Si cells [27] with a nominal capacity C_{nom} of 2.5 Ah, a mass of 45 g, a voltage range of 2.5 to 4.2 V, a nominal voltage U_{nom} of 3.6 V, maximum current rate of 8C for continuous discharge and 1.6C for continuous charge, temperature range going from 0 to 50 °C in charge and from -20 to 70 °C in discharge [28]. Each one of these cells has a different state of health ($SOH = C/C_{nom}$, where C is the cell capacity at the time of the test and C_{nom} is the nominal capacity):

- Cell A : SOH 100%.
- Cell B : SOH 95%. Mixed aging conditions, mostly cycling. This cell aged during electrical characterization tests, such as EIS, GITT (Galvanostatic Intermittent Titration Technique) and continuous charge / discharge. The test temperatures varied between 0 °C and 50 °C, with the maximum cell temperature reaching 70 °C. The current rates varied from C/2 to 1C in charge and from 1C to 5C in discharge. The tests that contributed most to aging were probably continuous discharges at 3C and 5C, with extreme temperatures (0 °C and 50 °C). The cycling current rates varied between C/2 and 5C for room temperatures going from 0 °C to 50 °C, with maximum cell temperature reaching 70 °C.
- Cell C : SOH 87%. Calendar aging at 60 °C and SOC 100% during 55 days. Fig. 2 shows how its capacity changed over time. It is important to notice that this cell aged very fast because of the high temperature. Another cell of the same reference, aged at 50 °C, reached the same final capacity after around 1 year.

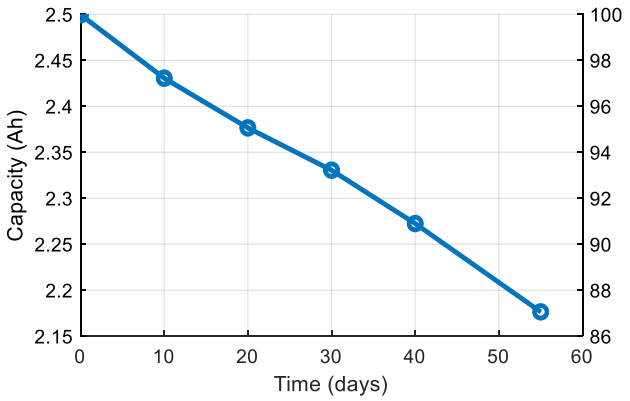

Figure 2: Capacity of cell C over time during calendar aging

A Bio-Logic system was used for tests (VSP-300) with a 20 A booster. The precision of this device is 0.1% of its full scale. Besides, the cells were placed into a climatic chamber to control their temperatures.

The experimental protocol, applied at three different temperatures (25 °C, 0 °C, -10 °C) consists of three main parts:

1. Initialization
2. EIS
3. Current pulses in charge and discharge

For the first part, the temperature was set to 25 °C, the cell was fully discharged and then charged up to 2 Ah (80% of the nominal capacity).

For the second part of the protocol, the climatic chamber was adjusted to perform the tests at the temperatures mentioned above. The EIS tests consists of applying a sine current wave to the cell and measuring its voltage variation in order to compute its impedance. This test was performed from 10 kHz to 10 mHz at C/5 and C/50. The reason for using different currents is that the lower the current, the more reasonable it is to admit that the impedance is identified at zero current, especially at very low temperatures. However, such low currents tend to cause imprecise measurements at higher frequencies, where series resistance is identified. So, when processing the EIS results, the spectrum obtained with a C/5 current was used to identify the series resistance (medium to high frequencies), while the spectrum obtained with a C/50 current was used to identify the surface resistance (low frequencies). This is presented in Fig. 3 and detailed in section 2.3.1.

The third part consists of current pulses of 20 seconds followed by a 30 minutes pause around SOC 80%. The measurements were sampled every 500 ms and every 1 mV variation. By analyzing the variation of the

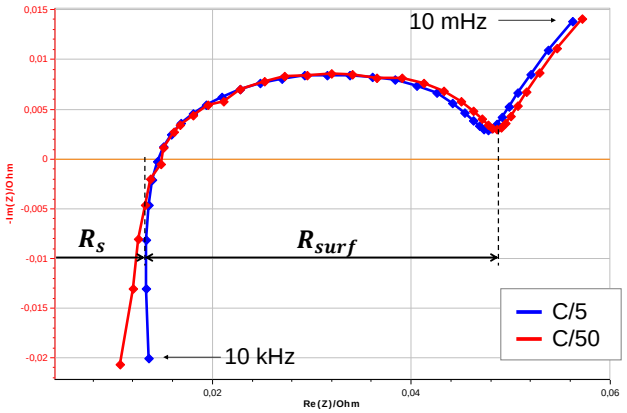

Figure 3: Identification of R_s and R_{surf} at near-zero current from an impedance spectrum (cell A tested at 0 °C, from 10 kHz fo 10 mHz with 6 points per decade)

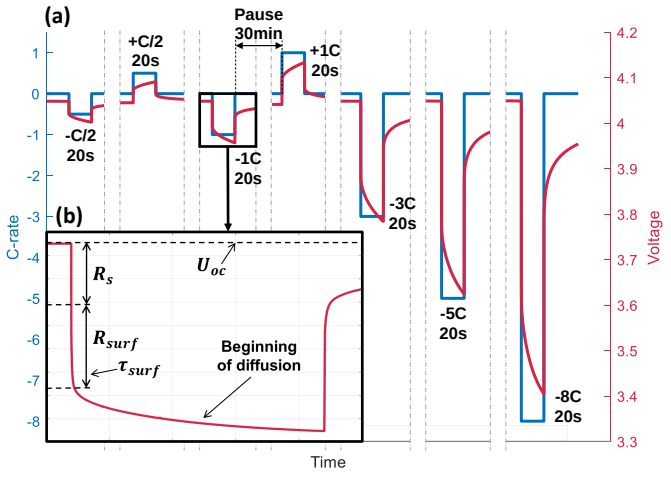

Figure 4: (a) Current pulses protocol and (b) identification of the parameters of the electrical model from the voltage response to a current pulse

voltage during the current pulses, we can extract information about the impedance of the cell. The following currents were tested: -C/2, -1C, -3C, -5C, -8C, +C/2 and +1C, the pulses in charge being applied only at 25 °C to avoid lithium-plating, specially in the case of the aged cells presenting a very high impedance. For the other temperatures, the charge current was limited to C/10. This protocol is presented in Fig. 4. The charges between the pulses at -3C, -5C and -8C were omitted to make the figure clearer, but they were done at C/2 (25 °C) or C/10 (0 °C and 10 °C) and recharged the same amount of *Ah* that had been discharged during the previous pulse.

This part of the protocol took 14.5 hours per cell for a total of 17 experimental points, i.e. approximately 51 minutes per point, while the protocol proposed by Damay *et al.* [12] took 150 hours for 70 conditions tested, i.e. 2 hours and 8 minutes per point. In his protocol, the current pulses were longer because the same tests were used in another study where it was important to accurately identify the diffusion parameters. With longer pulses, the rest time also had to be longer in order to achieve voltage and temperature equilibrium. The protocol proposed in the present work therefore represents a considerable time saving. The rest time could even be reduced to 15 minutes instead of 30 for current rates inferior to 3C, since temperature and voltage were already stable within this period. This would represent an additional gain of 4.5 hours.

2.3. Parameters identification

When characterizing the electrical model, the OCV and the series resistance may be determined first, then the other four parameters are identified simultaneously by fitting.

It is assumed that the series resistance does not depend on the current, so it can be determined from the EIS tests. The surface resistance for a near zero current can also be identified from EIS. The remaining parameters, including the surface resistance for currents different from near zero, require current pulses tests to be identified.

2.3.1. Identification from EIS tests

The impedance obtained from an EIS tests is presented in a Nyquist plot, with the real part of its value on the x-axis and the negative of its imaginary part on the y-axis.

R_s and R_{surf} can be determined as represented in Fig. 3. The series resistance R_s corresponds to the minimum real value of the impedance spectrum. The sum of the series and surface resistances is obtained from the real value of the impedance between the semi-circle and the slope (related to diffusion phenomena), where the imaginary part of the impedance reaches a local minimal value.

We found that R_s was more precisely determined at C/5, but we used a lower current for determining R_{surf} to be in accordance with a near-zero current assumption.

2.3.2. Identification from current pulses tests

For this study, the OCV during each pulse is identified by measuring the voltage at the beginning and at the end (after 30 minutes of rest) of the pulse and interpolating these two values. Next, the overvoltage ΔU is calculated by subtracting the OCV from the cell voltage and then fitted to find the remaining parameters using the function fmincon on Matlab using a loss function such as the root mean square error (RMSE). It is modeled by the following equation:

$$\Delta\hat{U}(t) = \left[R_s + R_{surf}\left(1 - \exp\left(-\frac{t}{\tau_{surf}}\right)\right) + \sum_{i=1}^{n} R_{diff,i}\left(1 - \exp\left(-\frac{t}{\tau_{diff,i}}\right)\right)\right] I(t) \quad (6)$$

where n is the number of diffusion circuits. We opted for 20 for this study, so that the time constants of the last circuits are sufficiently small to ensure a good accuracy in the beginning of the pulse, where the dynamics are fast.

The surface resistance can be determined from the EIS tests as explained in section 2.3.1. Fig. 4 shows the voltage response to a current pulse and gives some indication of which part corresponds to each parameter.

3. Separating SEI and charge transfers contributions to surface resistance

After presenting the electrical model of the cell and the identification of its parameters, we can focus on the main subject of the present article : the surface resistance. In this section, we are going to recall the modeling of charge transfers and SEI layer contributions to the surface resistance as a function of temperature and current, as proposed by Damay *et al.* [12].

The relation between the cell current I and the charge transfers voltage U_{ct} is based on the Butler-Volmer law [29]:

$$I = I_0 \left[\exp\left(\frac{(1-\beta)F}{R\,T} U_{ct} \right) - \exp\left(\frac{-\beta F}{R\,T} U_{ct} \right) \right] \quad (7)$$

where I_0 is the exchange current $[A]$, related to the charge transfer phenomena, β is the transfer coefficient, R is the universal gas constant $[J/(mol \cdot K)]$, T is the temperature $[K]$ ans F is the Faraday constant $[s \cdot A/mol]$.

Assuming that the charge transfers coefficient β is equal to 0.5 and knowing that $U_{ct} = U_{surf} - I \cdot R_{SEI}$ [29], the surface resistance can be isolated to find its dependence law on current:

$$R_{surf}(I) = \frac{U_{surf}}{I} = R_{SEI} + \frac{2\,R\,T}{F\,I} \operatorname{asinh}\left(\frac{I}{2\,I_0} \right) \quad (8)$$

It was demonstrated that R_{SEI} and I_0 are dependent on the temperature in accordance to the Arrhenius Law [3, 4, 12, 30]. In this work, the Arrhenius Law was normalized to display the parameters values at 25 °C. This brings the final R_{surf} equation below:

$$R_{surf}(I,T) = R_{SEI}(25°C) \times \exp\left(\frac{E_{a,SEI}}{k_B} \left(\frac{1}{T} - \frac{1}{298} \right) \right) + \frac{2\,R\,T}{F\,I} \operatorname{asinh}\left(\frac{I}{2\,I_0(25°C)} \exp\left(\frac{E_{a,I_0}}{k_B} \left(\frac{1}{T} - \frac{1}{298} \right) \right) \right) \quad (9)$$

where R_{SEI} is the resistance of the SEI layer at 25 °C $[\Omega]$, $E_{a,SEI}$ and E_{a,I_0} are the activation energies of the considered reactions $[eV]$ and k_B is the Boltzmann constant $[eV/K]$. The first term expresses the contribution of the SEI while the second expresses the contribution of the charge transfers. The parameters to be found are $R_{SEI}(25°C)$, $E_{a,SEI}$, $I_0(25°C)$ and E_{a,I_0}.

For a near zero current, the second term in equation 9 tends to equation 10, which corresponds to the classical electrochemical definition of charge transfers resistance [3, 4].

$$R_{ct,0}(T) = \frac{R\,T}{F\,I_0(T)} \quad (10)$$

4. Results and discussion

4.1. Fitting the model to the experimental data

After determining the value of R_{surf} for every test condition, the RMSRE (Root Mean Squared Relative Error) was used as the loss function to fit the model described in (9) to the experimental values. In a first step, the model was fitted for each SOH independently, each parameter being free to vary. In a second step, it was fitted with the activation energies kept constant for every state of health, since they depend on the chemical reactions occurring in the cell and these reactions are the same regardless of its state of health. This second approach leaves us with only two parameters to be found in each case, $R_{SEI}(25°C)$ and $I_0(25°C)$. The results obtained with the first approach (variable activation energies) are presented in section 4.1.2 and those obtained with the second approach (constant activation energies) are presented in section 4.1.3.

4.1.1. Definition of an equivalent activation energy for the charge transfers resistance

As indicated, the activation energy of a reaction is assumed to be independent of the state of health of the cell, since the chemical reaction is the same. However, in our model, the positive and negative electrodes are simplified into one single electrode. This should not affect $E_{a,SEI}$, as the SEI is only formed on the negative electrode, or at least we can neglect this phenomenon over the positive. However, the charge transfers take place on both positive and negative electrodes. Therefore, E_{a,I_0} can be expected to change with aging, depending on how the charge transfers resistances of each electrode increase.

To better understand it, we can calculate the equivalent activation energy for $R_{ct}(T)$. The thermal dependence of the positive (index P) and negative (index N) charge transfers resistances can be expressed as:

$$\begin{aligned} R_{ct,P}(T) &= R_{ct,P}(T_{ref}) \exp\left(\frac{E_{a,P}}{k_B} \left(\frac{1}{T} - \frac{1}{T_{ref}} \right) \right) \\ R_{ct,N}(T) &= R_{ct,N}(T_{ref}) \exp\left(\frac{E_{a,N}}{k_B} \left(\frac{1}{T} - \frac{1}{T_{ref}} \right) \right) \end{aligned} \quad (11)$$

where T_{ref} is a reference temperature.

For simplicity, the activation energies are denoted $E_{a,P}$ and $E_{a,N}$, but they are equivalent to $E_{a,I_0,P}$ and $E_{a,I_0,N}$.

The equivalent resistance R_{ct} is the sum of $R_{ct,P}$ and $R_{ct,N}$. To develop the exponentials, we can use Taylor's theorem :

$$\exp(x) \approx 1 + \frac{x}{1!} + \frac{x^2}{2!} + ... + \frac{x^n}{n!} \quad (12)$$

For $x \approx 0$, we can admit that $\exp(x) \approx 1+x$. Then, if $1/T$ is close to $1/T_{ref}$, the sum of the two resistances gives:

$$\begin{aligned} R_{ct}(T) &= R_{ct,P}(T_{ref})\left(1+\frac{E_{a,P}}{k_B}\left(\frac{1}{T}-\frac{1}{T_{ref}}\right)\right)+R_{ct,N}(T_{ref})\left(1+\frac{E_{a,N}}{k_B}\left(\frac{1}{T}-\frac{1}{T_{ref}}\right)\right) \\ &\approx R_{ct,P}(T_{ref})+R_{ct,N}(T_{ref})+\frac{1}{k_B}\left(\frac{1}{T}-\frac{1}{T_{ref}}\right)\left(R_{ct,P}(T_{ref})E_{a,P}+R_{ct,N}(T_{ref})E_{a,N}\right) \\ &\approx \left(R_{ct,P}(T_{ref})+R_{ct,N}(T_{ref})\right)\left(1+\left(\frac{R_{ct,P}(T_{ref})E_{a,P}+R_{ct,N}(T_{ref})E_{a,N}}{R_{ct,P}(T_{ref})+R_{ct,N}(T_{ref})}\right)\frac{1}{k_B}\left(\frac{1}{T}-\frac{1}{T_{ref}}\right)\right) \end{aligned} \tag{13}$$

which can be written as:

$$R_{ct}(T) \approx R_{ct}(T_{ref})\exp\left(\frac{E_a}{k_B}\left(\frac{1}{T}-\frac{1}{T_{ref}}\right)\right) \tag{14}$$

where:

$$R_{ct}(T_{ref}) = R_{ct,P}(T_{ref}) + R_{ct,N}(T_{ref}) \tag{15}$$

$$E_a \approx \frac{R_{ct,P}(T_{ref})E_{a,P}+R_{ct,N}(T_{ref})E_{a,N}}{R_{ct,P}(T_{ref})+R_{ct,N}(T_{ref})} \tag{16}$$

The closer the term inside the exponential in equation (14) is to zero, the more accurate the approximation will be. For a temperature range going from -20 °C to 70 °C, for example, this term varies at most between 6.9 and -5.1 (for a pessimistic activation energy of 1). Depending on the required accuracy, this may lead to some errors for the extreme operating temperatures, but the error should be acceptable pour most of the use cases.

Equation (16) shows that the equivalent activation energy of two charge transfers resistances depends on the relative values of these resistances as a weighted average. Thus, the equivalent activation energy always tends towards the activation energy of the highest resistance, as it will be shown in the next section. When a battery ages, the charge transfers resistances of the positive and negative electrodes may increase in different proportions, as stated in the introduction of this paper. Consequently, we expect the equivalent activation energy to change with aging.

4.1.2. Results with a variable equivalent activation energy

Fig. 5a shows the fitting results obtained when we allow the activation energies to vary. Fig. 5b shows the contributions of SEI layer and charge transfers to the overall surface resistance. The values of the parameters from (9) are presented in Tab. 1. The activation energy related to the SEI layer ($E_{a,SEI}$) does not change significantly with the state of health, which is consistent with the hypothesis of negligible SEI at the positive electrode. The activation energy related to the charge transfers, on the other hand, decreases from 0.87 to 0.62 eV (-30%) between SOH 100% and 87%.

The activation energy $E_{a,SEI}$ is a little lower than the values presented in literature (0.59 eV found by Damay *et al.* [12] and 0.52 eV found by Pinson *et al.* [31]), which can be explained by the differences in the composition of the SEI layer for cells of different chemistries. The value of E_{a,I_0} at SOH 100% is close to that proposed by Damay *et al.* [12], 0.81 eV, suggesting that the equivalent charge transfers resistance might be dominated by the charge transfers of the negative electrode. As the battery ages, E_{a,I_0} gets closer to the activation energies of charge transfers for NMC and NCA electrodes, respectively 0.3-0.4 eV and 0.5 eV as reported by Xu *et al.* [32] and Jow *et al.* [33]. As discussed in section 4.1.1, this suggests that the charge transfers resistance of the positive electrode has increased compared to that of the negative electrode. These results are quite promising and they are consistent with the results of Stiaszny *et al.* [16], as stated in the introduction of this paper.

Table 1: Model parameters (variable activation energies)

Parameter		**SOH 100%**	**SOH 95%**	**SOH 87%**
$\mathbf{R_{SEI}(25°C)}$	$[m\Omega]$	4.52	5.48	6.79
$\mathbf{E_{a,SEI}}$	$[eV]$	0.38	0.40	0.37
$\mathbf{I_0(25°}C\mathbf{)}$	$[A]$	30.8	6.31	2.06
$\mathbf{E_{a,I_0}}$	$[eV]$	0.87	0.72	0.62
$\mathbf{R_{ct_0}(25°C)}$	$[m\Omega]$	0.83	4.07	12.45
RMSRE	[%]	3.70	3.94	5.36
RMSE	$[m\Omega]$	1.97	2.81	5.82

4.1.3. Results with a constant equivalent activation energy

From a diagnosis point of view, it is more rigorous to redetermine all parameters of (9) as the cell ages. However, this means that all tests must be repeated for each state of health. From an engineering point of view, it would be interesting to have less parameters to determine. This is why the second method we propose consists in choosing activation energies that are approximately coherent for all states of charge and only updating $R_{SEI}(25°C)$ and $I_0(25°C)$. We decided to adopt the activation energies identified at

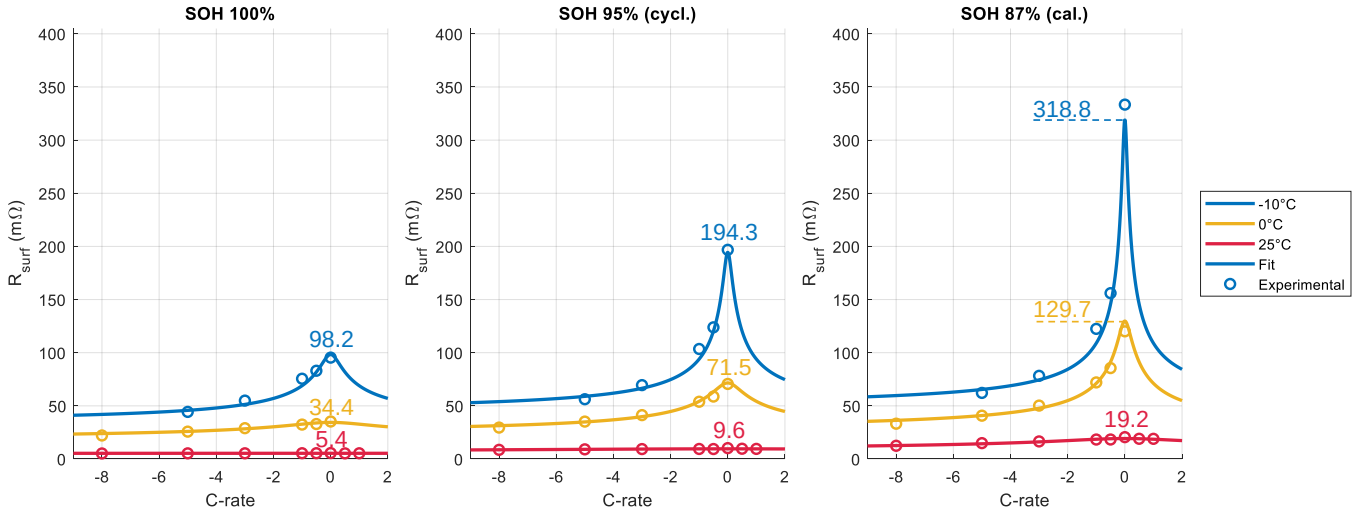

(a) Experimental points and fitting results for the surface resistance

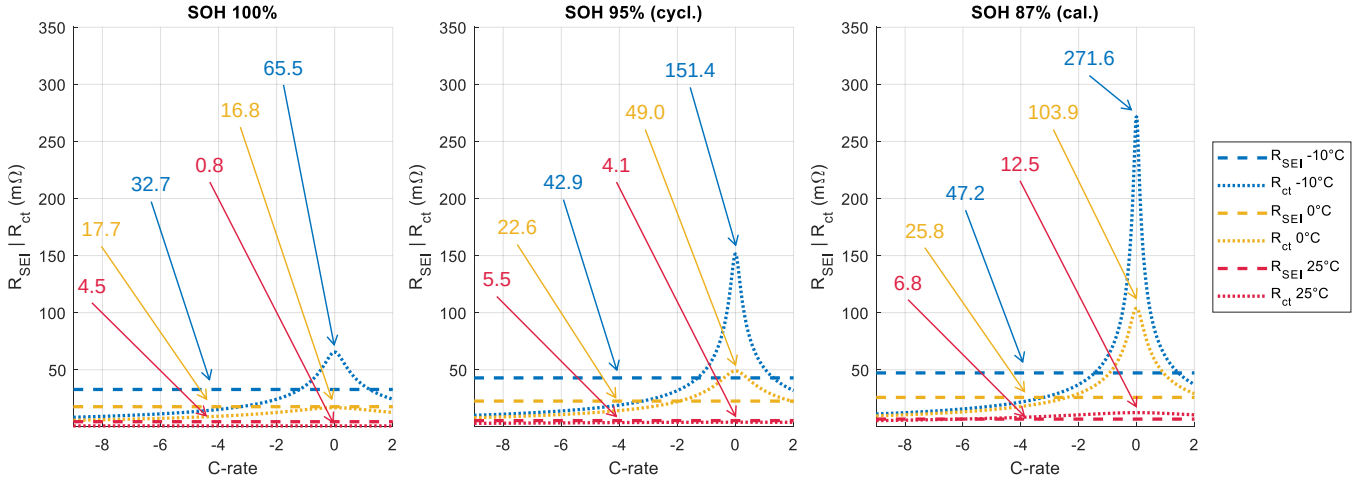

(b) Separation of SEI layer and charge transfers contributions

Figure 5: Fitting results at different states of health using the variable activation energies

SOH 95%, since it is an intermediate between SOH 100% and 87%.

Fig. 6a shows the fitting results obtained when the activation energies are forced to be the same for all states of health. The values of the parameters from (9) are presented in Tab. 2. Fig. 6b shows the contributions of SEI layer and charge transfers to the overall surface resistance. This simplified method works well for most of the operating conditions tested, except for near zero current at -10 °C, which will rarely be the operating condition of our application. To improve accuracy in this condition, the RMSE (Root Mean Squared Error) could be used as the loss function instead of the RMSRE. It would reduce the absolute error at low temperature and current, to the detriment of the relative error at ambient temperature.

Table 2: Model parameters (same activation energies)

Parameter		**SOH 100%**	**SOH 95%**	**SOH 87%**
$\mathbf{R_{SEI}(25°C)}$	$[m\Omega]$	3.88	5.42	6.56
$\mathbf{E_{a,SEI}}$	$[eV]$		0.40	
$\mathbf{I_0(25°C)}$	$[A]$	15.68	6.24	2.69
$\mathbf{E_{a,I_0}}$	$[eV]$		0.72	
$\mathbf{R_{ct_0}(25°C)}$	$[m\Omega]$	1.64	4.12	9.53
RMSRE	[%]	5.17	3.94	12.78
RMSE	$[m\Omega]$	3.18	2.76	17.20

4.2. Evolution of surface resistance for damaged cells

The results presented in Tab. 1 and Tab. 2 show that both SEI and charge transfers resistance increased during cycling and calendar conditions. In both cases,

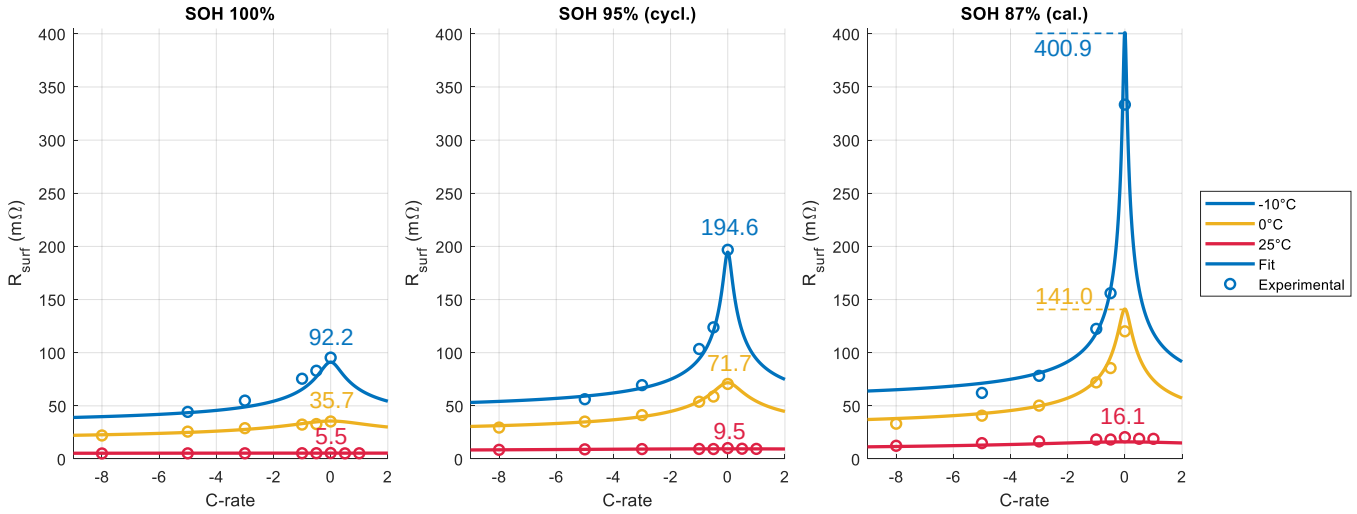

(a) Experimental points and fitting results for the surface resistance

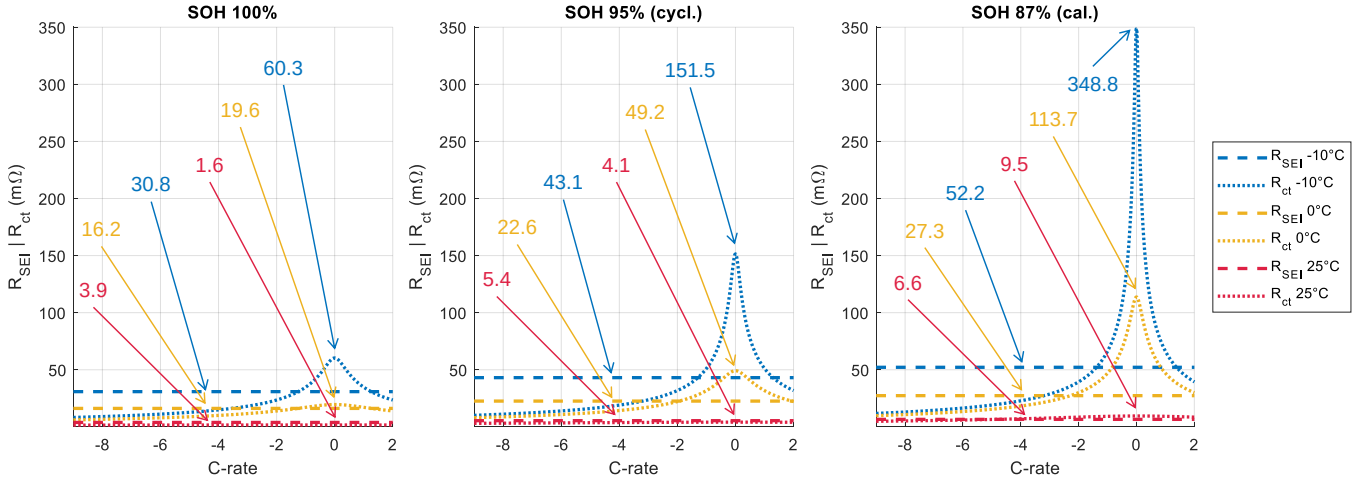

(b) Separation of SEI layer and charge transfers contributions

Figure 6: Fitting results at different states of health using the same activation energies

the increase factor of $R_{ct_0}(25°C)$ is higher than that of $R_{SEI}(25°C)$. For SOH 87%, for example, $R_{SEI}(25°C)$ is multiplied by 1.5 (with variable activation energies, 1.7 otherwise) while $R_{ct_0}(25°C)$ is multiplied by 15 (with variable activation energies, 5.8 otherwise). Both aging conditions appear to trigger mechanisms that contribute in a similar way to the thickening of the SEI layer and to a decrease of the charge transfers efficiency across the electrodes surfaces. The interpretation of these equivalent resistances evolution has to be done carefully, because several causes may lead to their increase. More information would be required to provide a solid explanation to this macroscopic degradation.

In references [13, 14, 15, 16] that concern studies in different calendar and cycling conditions, the SEI resistance increases at most by a factor 3.5 and the charge transfers resistance increases at most by a factor 10. These strong variations are consistent with our results. The increase in SEI resistance for the cell that aged during characterization tests might be justified by long periods at 50 °C during these tests, which seem to have a calendar contribution.

The results we obtained, specially using the method where the activation energies vary, opens doors for further study about the separation of the charge transfers resistances of each electrode. It would be necessary to have a good knowledge of the activation energies at each electrode so that the two resistances could then be decoupled using equations (14) and (16).

5. Conclusions

The presented method, originally proposed and applied to an LFP / graphite cell, was successfully transposed to an NCA+NMC / graphite+Si cell. EIS and pulses tests are combined to bring a good representation of the nonlinear behavior of charge transfer and SEI resistances re-

garding current and temperature. This allows for the separation of SEI and charge transfers resistances, plus their activation energies, even if these phenomena contributions are not clearly distinguishable in the EIS spectrum.

The evolution of SEI and charge transfers resistances (respectively R_{SEI} and R_{ct}) was characterized for degraded cells and we showed that their variations are consistent with literature. We found that charge transfers resistance had increased with both cycling and calendar degradations. SEI resistance increased in both conditions as well, probably due to the high temperatures to which the cells were subjected in both cases. This suggest that this approach is well-adapted for the diagnosis of SEI and charge transfer equivalent resistance, making it a promising tool for future aging studies.

We observed that at 25 °C, the two resistances are balanced. At low temperatures, R_{ct} increases significantly as current tends towards zero, becoming much higher than R_{SEI}. Besides, this effect is accentuated with degraded cells. As the current increases, R_{ct} tends to zero, while R_{SEI} does not change, making it a major contribution at high power. Please note that these relations may vary for different chemistries.

We showed two possibilities to recalibrate the proposed model with degraded cells. The first method consists in updating all the parameters. More specifically, we considered a variable equivalent activation energy for charge transfers, which appears to be more rigorous from a diagnosis point of view. For a simulation purpose, this first method would already allow the number of characterization tests to be reduced compared to the use of lookup tables. Concerning highly non-linear behaviors such as the surface resistance, lookup tables require a high resolution in order to give precise results (that is many values for different current and temperature conditions). Using a non-linearity model like the one proposed in this work requires to test fewer operating points of the battery since the non-linear behavior can be reproduced by the analytical equation.

The second recalibration method, in which we considered a constant equivalent activation energy for charge transfers, only have two parameters to be determined ($R_{SEI}(25°C)$ and $I_0(25°C)$). It is more practical from an engineering point of view, because it would be possible to reduce the number of characterization tests even further, since only two parameters need to be updated.

We also proposed an explanation for the evolution of the charge transfers activation energy when a battery ages. We suggest that it should be considered as an apparent activation energy, that depends on the relative contributions of both charge transfer resistances at the positive and negative electrodes. For instance, in this study, our results suggest that the charge transfer resistance of the positive electrode has increased faster than the one of the negative electrode during aging.

6. Perspectives

It may be possible to embed the proposed modeling method into a BMS (Battery Management System) in order to do an on-line recalibration of the surface resistance as the battery ages. It could be done by using current pulses at different temperatures during operation. In this case, the EIS test could be replaced by a very low current pulse. However, this possibility should be investigated based on system limitations, such as sampling rate, sensors accuracy, among other factors.

Furthermore, our results are potentially a starting point for a study about the separation of the charge transfers resistances of the two electrodes through the equivalent activation energy. This could allow for even finer diagnostics, perhaps uncovering operating limits of the cell.

We also propose that our method be tested on a larger volume of data to assess its capabilities. In particular, it would be interesting to test cells at different states of health, but aged in the same way, and compare the results obtained when the aging mode changes.

Acknowledgements

This work was funded by Safran Electrical & Power and the ANRT (National Association for Research and Technology) as part of a CIFRE PhD thesis (n° 2019/1062).

Declaration of competing interest

The authors declare that they have no known competing financial interests or personal relationships that could have appeared to influence the work reported in this paper.

References

[1] M. Mastali, M. Farkhondeh, S. Farhad, R. A. Fraser, M. Fowler, Electrochemical modeling of commercial $LiFePO_4$ and graphite electrodes: Kinetic and transport properties and their temperature dependence, Journal of The Electrochemical Society 163 (2016) A2803–A2816.

[2] X. Han, M. Ouyang, L. Lu, J. Li, Simplification of physics-based electrochemical model for lithium ion battery on electric vehicle. Part II: Pseudo-two-dimensional model simplification and state of charge estimation, Journal of Power Sources 278 (2015) 814–825.

[3] M. Takahashi, S.-I. Tobishima, K. Takei, Y. Sakurai, Reaction behavior of $LiFePO_4$ as a cathode material for rechargeable lithium batteries, Solid State Ionics 148 (2002) 283–289.

[4] M. Ecker, T. K. D. Tran, P. Dechent, S. Käbitz, A. Warnecke, D. U. Sauer, Parameterization of a physico-chemical model of a lithium-ion battery, Journal of The Electrochemical Society 162 (2015) A1836–A1848.

[5] G. Dong, X. Zhang, C. Zhang, Z. Chen, A method for state of energy estimation of lithium-ion batteries based on neural network model, Energy 90 (2015) 879–888.

[6] J. Illig, M. Ender, T. Chrobak, J. P. Schmidt, D. Klotz, E. Ivers-Tiffée, Separation of charge transfer and contact resistance in $LiFePO_4$-cathodes by impedance modeling, Journal of The Electrochemical Society 159 (2012) A952–A960.

[7] J. Illig, M. Ender, A. Weber, E. Ivers-Tiffée, Modeling graphite anodes with serial and transmission line models, Journal of Power Sources 282 (2015) 335–347.
[8] D. Andre, M. Meiler, K. Steiner, H. Walz, T. Soczka-Guth, D. U. Sauer, Characterization of high-power lithium-ion batteries by electrochemical impedance spectroscopy. Part II: Modelling, Journal of Power Sources 196 (2011) 5349–5356.
[9] M. Juston, N. Damay, C. Forgez, G. Friedrich, S. Vivier, K. M. Mbeya, B. Vulturescu, Direct determination of a single battery internal resistances distribution using a heterogeneous model, Mathematics and Computers in Simulation 183 (2021) 20–33.
[10] M. Gholizadeh, F. R. Salmasi, Estimation of state of charge, unknown nonlinearities, and state of health of a lithium-ion battery based on a comprehensive unobservable model, IEEE Transactions on Industrial Electronics 61 (2014) 1335–1344.
[11] K. Onda, T. Ohshima, M. Nakayama, K. Fukuda, T. Araki, Thermal behavior of small lithium-ion battery during rapid charge and discharge cycles, Journal of Power Sources 158 (2006) 535–542.
[12] N. Damay, K. M. Mbeya, G. Friedrich, C. Forgez, Separation of the charge transfers and solid electrolyte interphase contributions to a battery voltage by modeling their non-linearities regarding current and temperature, Journal of Power Sources 516 (2021) 230617.
[13] D. N. Wong, D. A. Wetz, A. M. Mansour, J. M. Heinzel, The influence of high C-rate pulsed discharge on lithium-ion battery cell degradation, volume 2015-October, Institute of Electrical and Electronics Engineers Inc., 2015. 17.
[14] D. Wong, B. Shrestha, D. A. Wetz, J. M. Heinzel, Impact of high rate discharge on the aging of lithium nickel cobalt aluminum oxide batteries, Journal of Power Sources 280 (2015) 363–372. 63.
[15] P. S. Sabet, A. J. Warnecke, F. Meier, H. Witzenhausen, E. Martinez-Laserna, D. U. Sauer, Non-invasive yet separate investigation of anode/cathode degradation of lithium-ion batteries (nickel–cobalt–manganese vs. graphite) due to accelerated aging, Journal of Power Sources 449 (2020) 227369. 59.
[16] B. Stiaszny, J. C. Ziegler, E. E. Krauß, M. Zhang, J. P. Schmidt, E. Ivers-Tiffée, Electrochemical characterization and post-mortem analysis of aged $LiMn_2O_4$–NMC/graphite lithium ion batteries, Part II: Calendar aging, Journal of Power Sources 258 (2014) 61–75. 57.
[17] I. A. Jiménez Gordon, S. Grugeon, H. Takenouti, B. Tribollet, M. Armand, C. Davoisne, A. Débart, S. Laruelle, Electrochemical Impedance Spectroscopy response study of a commercial graphite-based negative electrode for Li-ion batteries as function of the cell state of charge and ageing, Electrochimica Acta 223 (2017) 63–73.
[18] N. Meddings, M. Heinrich, F. Overney, J. S. Lee, V. Ruiz, E. Napolitano, S. Seitz, G. Hinds, R. Raccichini, M. Gaberšček, J. Park, Application of electrochemical impedance spectroscopy to commercial Li-ion cells: A review, Journal of Power Sources 480 (2020).
[19] J. Illig, J. P. Schmidt, M. Weiss, A. Weber, E. Ivers-Tiffée, Understanding the impedance spectrum of 18650 $LiFePO_4$ cells, Journal of Power Sources 239 (2013) 670–679.
[20] F. Schipper, E. M. Erickson, C. Erk, J.-Y. Shin, F. F. Chesneau, D. Aurbach, Review—Recent Advances and Remaining Challenges for Lithium Ion Battery Cathodes, Journal of The Electrochemical Society 164 (2017) A6220–A6228.
[21] D. Pritzl, A. E. Bumberger, M. Wetjen, J. Landesfeind, S. Solchenbach, H. A. Gasteiger, Identifying Contact Resistances in High-Voltage Cathodes by Impedance Spectroscopy, Journal of The Electrochemical Society 166 (2019) A582–A590.
[22] J. N. Zhang, Q. Li, Y. Wang, J. Zheng, X. Yu, H. Li, Dynamic evolution of cathode electrolyte interphase (CEI) on high voltage $LiCoO_2$ cathode and its interaction with Li anode, Energy Storage Materials 14 (2018) 1–7.
[23] S. Solchenbach, X. Huang, D. Pritzl, J. Landesfeind, H. A. Gasteiger, Monitoring SEI Formation on Graphite Electrodes in Lithium-Ion Cells by Impedance Spectroscopy, Journal of The Electrochemical Society 168 (2021) 110503.
[24] L. Gagneur, A. Driemeyer-Franco, C. Forgez, G. Friedrich, Modeling of the diffusion phenomenon in a lithium-ion cell using frequency or time domain identification, Microelectronics Reliability 53 (2013) 784–796.
[25] J. Huang, H. Ge, Z. Li, J. Zhang, An Agglomerate Model for the Impedance of Secondary Particle in Lithium-Ion Battery Electrode, Journal of The Electrochemical Society 161 (2014) E3202–E3215.
[26] E. Kuhn, C. Forgez, P. Lagonotte, G. Friedrich, Modelling Ni-MH battery using Cauer and Foster structures, Journal of Power Sources 158 (2006) 1490–1497.
[27] M. J. Lain, J. Brandon, E. Kendrick, Design strategies for high power vs. high energy lithium ion cells, Batteries 5 (2019).
[28] Specification of product - Lithium-ion recheargeable cell for power tools, model name: INR18650-25R, Samsung SDI, 2014. Version No. 1.0.
[29] M. Farkhondeh, C. Delacourt, Mathematical modeling of commercial $LiFePO_4$ electrodes based on variable solid-state diffusivity, Journal of The Electrochemical Society 159 (2011) A177–A192.
[30] M. Park, X. Zhang, M. Chung, G. B. Less, A. M. Sastry, A review of conduction phenomena in Li-ion batteries, Journal of Power Sources 195 (2010) 7904–7929.
[31] M. B. Pinson, M. Z. Bazant, Theory of SEI formation in rechargeable batteries: Capacity fade, accelerated aging and lifetime prediction, Journal of The Electrochemical Society 160 (2013) A243–A250.
[32] J. Xu, S. L. Chou, Q. F. Gu, H. K. Liu, S. X. Dou, The effect of different binders on electrochemical properties of $LiNi_{1/3}Mn_{1/3}Co_{1/3}O_2$ cathode material in lithium ion batteries, Journal of Power Sources 225 (2013) 172–178.
[33] T. R. Jow, M. B. Marx, J. L. Allen, Distinguishing Li + charge transfer kinetics at NCA/electrolyte and graphite/electrolyte interfaces, and NCA/electrolyte and LFP/electrolyte interfaces in Li-Ion cells, Journal of The Electrochemical Society 159 (2012) A604–A612.